arXiv:cond-mat/0309481v1 [cond-mat.mtrl-sci] 21 Sep 2003

# Free energy and configurational entropy of liquid silica: fragile-to-strong crossover and polyamorphism

Ivan Saika-Voivod,[1,2] Francesco Sciortino,[2] and Peter H. Poole[1,3]

[1] *Department of Applied Mathematics, University of Western Ontario, London, Ontario N6A 5B7, Canada*
[2] *Dipartimento di Fisica and Istituto Nazionale per la Fisica della Materia, Universita' di Roma La Sapienza, Piazzale Aldo Moro 2, I-00185, Roma, Italy*
[3] *Department of Physics, St. Francis Xavier University, Antigonish, Nova Scotia B2G 2W5, Canada*

(Dated: February 2, 2008)

Recent molecular dynamics (MD) simulations of liquid silica, using the "BKS" model [Van Beest, Kramer and van Santen, Phys. Rev. Lett. **64**, 1955 (1990)], have demonstrated that the liquid undergoes a dynamical crossover from super-Arrhenius, or "fragile" behavior, to Arrhenius, or "strong" behavior, as temperature $T$ is decreased. From extensive MD simulations, we show that this fragile-to-strong crossover (FSC) can be connected to changes in the properties of the potential energy landscape, or surface (PES), of the liquid. To achieve this, we use thermodynamic integration to evaluate the absolute free energy of the liquid over a wide range of density and $T$. We use this free energy data, along with the concept of "inherent structures" of the PES, to evaluate the absolute configurational entropy $S_c$ of the liquid. We find that the temperature dependence of the diffusion coefficient and of $S_c$ are consistent with the prediction of Adam and Gibbs, including in the region where we observe the FSC to occur. We find that the FSC is related to a change in the properties of the PES explored by the liquid, specifically an inflection in the $T$ dependence of the average inherent structure energy. In addition, we find that the high $T$ behavior of $S_c$ suggests that the liquid entropy might approach zero at finite $T$, behavior associated with the so-called Kauzmann paradox. However, we find that the change in the PES that underlies the FSC is associated with a change in the $T$ dependence of $S_c$ that elucidates how the Kauzmann paradox is avoided in this system. Finally, we also explore the relation of the observed PES changes to the recently discussed possibility that BKS silica exhibits a liquid-liquid phase transition, a behavior that has been proposed to underlie the observed polyamorphism of amorphous solid silica.

PACS numbers: 64.70.Pf, 66.20.+d, 65.40.Gr, 65.20+w

## I. INTRODUCTION

Liquid silica is the archetypal "strong liquid," that is, a liquid whose viscosity $\eta$ and other measures of relaxation follow closely an Arrhenius behavior, $\log \eta \sim 1/T$ [1, 2], where $T$ is the temperature. For most liquids, $\eta$ increases significantly faster than an Arrhenius law as $T$ approaches the glass transition temperature $T_g$; these liquids are referred to as "fragile."

Strong liquids such as silica are important as glass-forming systems. In a strong liquid, $\eta$ varies less rapidly with $T$ near $T_g$, compared to a fragile liquid. As a consequence, a strong liquid can be held in a desired range of $\eta$ over a wider range of $T$ than a fragile liquid. As every glassblower knows, this makes silica-based systems easier to manipulate just above $T_g$ than any other commonly available liquid.

The fundamental origins of strong behavior in glass-forming liquids is also a subject of continuing interest. We note in particular two recent developments. First, computer simulation work of Horbach and Kob [3] using the "BKS" model of silica [4] has demonstrated that at high $T$, the model liquid exhibits fragile behavior, and then crosses over to a regime of strong behavior upon cooling. The work of La Nave and coworkers, based on instantaneous normal mode analysis, has shown that such a crossover is connected to a progressive reduction in the number of diffusive directions in phase space accessed by the system [5]. Such a "fragile-to-strong crossover" (FSC) may be a general mechanism underlying the emergence of strong behavior, and has since been studied for a number of systems [6]. We note that a crossover from a super-Arrhenius to Arrhenius dynamics may be a general feature of liquids around the so-called mode-coupling temperature [7], as is appearing to emerge in recent numerical studies, thanks to the the larger dynamical window made available by current computational power [8, 9, 10]. However, the $T$ region where equilibrium simulations can be performed is still limited, and does not allow for a precise statement of the $T$-dependence below the crossover temperature, as required to make final contact with models for the glass transition [11, 12, 13].

Second, a growing body of computer simulation research has established the importance of the potential energy landscape or surface (PES) for understanding the dynamics of liquids near $T_g$ [9, 14, 15, 16, 17, 18, 19, 20, 21, 22, 23, 24, 25]. The PES refers specifically to $\mathcal{U}$, the instantaneous potential energy hypersurface of the system, expressed as a function of the $3N$ coordinates $q_i$ that specify the positions of the $N$ atoms of the system; i.e. $\mathcal{U} = \mathcal{U}(q_1, q_2, ..., q_{3N})$. The properties and topology of the PES have been carefully studied in the above cited works, predominantly in the case of fragile liquids, resulting in important insights into the equilibrium [26] and out-of-equilibrium [27, 28] thermodynamics

of supercooled states, and the connection between thermodynamics and transport propertie [21, 29]. However, the relationship of the PES to the dynamic properties of strong liquids is less well understood. In this paper, our focus is to clarify this relationship, and in particular, to determine if the FSC proposed for liquid silica can be connected to properties of the PES.

Following previous studies of fragile liquids, our approach is to apply the "inherent structure" formalism of Stillinger and Weber [15] to molecular dynamics (MD) computer simulation data obtained for the BKS model of liquid silica. In this approach, the PES is partitioned into basins associated with the local minima of $\mathcal{U}$ [14, 15, 16]. Each minimum corresponds to a particular configuration of atoms and is called an inherent structure (IS). We denote by $e_{IS}$ the average potential energy of the IS's associated with the basins sampled by the equilibrium liquid at a given $T$ and volume $V$. An IS and its energy can be obtained in computer simulation by carrying out a local minimization of $\mathcal{U}$ starting from an equilibrium liquid configuration.

As we will describe in detail below, the evaluation of $e_{IS}$, combined with free energy calculations, allows us to calculate the configurational entropy, $S_c$, of the system [9, 18, 20, 21, 24]. $S_c$ determines the number of distinct configurations explored by the system, in this case the basins of the PES. In a liquid, diffusion is associated with the exploration by the system of different basins of the PES. The work of Adam and Gibbs (AG) predicts a relationship (in the low $T$ limit) between the characteristic relaxation time of the system and $S_c$ [30]. The AG relation has been recently derived in a novel way [12]. Generalizing the AG relation to the diffusion coefficient $D$, the AG relation can be written as,

$$\frac{D}{T} = \mu_0 \exp\left(-\frac{A}{TS_c}\right), \tag{1}$$

where $\mu_0$ and $A$ are presumed to be constant with respect to $T$. In the context of liquid silica, an interesting test of the robustness of the AG relation is possible by checking if Eq. 1 is obeyed throughout the region in which the FSC occurs. If so, the AG relation then provides a basis for connecting transport behavior (quantified by $D$) to the properties of the PES (quantified by $S_c$ and $e_{IS}$).

In a recent letter [31], we showed that liquid BKS silica behaves in a manner that allows $S_c$ to be calculated from $e_{IS}$, and that $D$ and $S_c$ are related as predicted by the AG relation. We were thereby able to show that the FSC in liquid silica is associated with a change in the $T$ dependence of $e_{IS}$, i.e. a change in the nature of the PES explored by the system as $T$ decreases. We also found that this observation in turn has implications for other behavior observed in BKS silica, in particular, the possible occurrence of a liquid-liquid transition, and the behavior of the liquid as related to the so-called Kauzmann paradox.

To reach such conclusions, extensive MD simulations are required over a wide range of $V$ and $T$, to calculate thermodynamic and transport properties, as well as careful examination of the IS properties. In addition, the absolute free energy of the liquid must be evaluated. In the present work, we provide a detailed description of the methods used to obtain the results summarized in Ref. [31], and also provide an expanded analysis and discussion of the results. This work is organized as follows. In Section II we describe our MD simulations, including the interaction potential used. Section III provides a detailed description of the techniques we use to evaluate $e_{IS}$, $S_c$, and the total free energy of the liquid. Section IV presents the results of these calculations and provides a discussion of their implications.

## II. MOLECULAR DYNAMICS SIMULATIONS

We carry out MD simulations at constant $V$. Most of our results are for a system of 444 Si atoms and 888 O atoms. A few simulations are carried out with a reduced number of particles (333 Si and 666 O atoms) in order to access longer physical times scales. Our MD simulation program is based on the "MDCSPC2" source code [32]. We also reproduce a subset of our results using a code we have written independently of MDCSPC2. Note that all molar quantities are reported here in moles of atoms.

Our model of atomic interactions in silica, denoted here as $\Phi_{BKS}$, is based on the BKS potential, modified in two ways. First, the BKS potential energy for both the Si-O and O-O interactions diverges unphysically to negative infinity at sufficiently small distances, allowing "fusion" events to occur during simulation of high $T$ systems. To prevent this, $\Phi_{BKS}$ consists of the standard BKS potential plus a short range term given by

$$4\epsilon_{\mu\nu}\left[\left(\frac{\sigma_{\mu\nu}}{r_{ij}}\right)^{30} - \left(\frac{\sigma_{\mu\nu}}{r_{ij}}\right)^{6}\right] \tag{2}$$

where $r_{ij}$ is the interatomic separation between an atom $i$ of species $\mu$, and an atom $j$ of species $\nu$. To choose the parameters $\epsilon_{\mu\nu}$ and $\sigma_{\mu\nu}$ (see Table I) we first identify the value $r_{ij} = r^*_{ij}$ at which the inflection of the standard BKS potential occurs, below which the divergence to negative infinity develops. The parameters are chosen so that the new potential increases monotonically, and without inflections, as $r_{ij}$ decreases for $r_{ij} < r^*_{ij}$; and so that the difference between the new and the old potentials is small for $r_{ij} > r^*_{ij}$. Similar approaches have been used in other works [33, 34].

The second modification to the standard BKS potential included in $\Phi_{BKS}$ relates to the treatment of longer range interactions. As is common in implementations of the BKS potential, we calculate the long range contributions to the Coulombic potential energy using the Ewald summation technique, with the dipole surface term set to zero [35]. The reciprocal space summation is carried out to a radius of six reciprocal lattice cell widths. In

this approach, the real space contributions to the BKS potential are usually cut off discontinuously at a specified distance, often chosen as $L/2$, where $L$ is the length of an edge of the simulation cell. However, we study systems over a wide range of density $\rho$, and we desire a potential for which the cut-off is independent of $L$. Also, for accurate determination of inherent structures, we wish to remove discontinuities in the potential energy arising from cut-offs, and to remove any $L$ dependence from long range corrections associated with the cut-off.

To achieve these goals, instead of discontinuously cutting off the real space potential contributions, we introduce a switching function. At a fixed distance $R_s = 0.77476$ nm the real space terms of the standard BKS potential are replaced by a 5th degree polynomial that tapers smoothly to zero over the range $R_s < r_{ij} < R_c$, where $R_c = 1$ nm. The polynomial coefficients and the value of $R_s$ are chosen so that the potential is continuous up to and including second derivatives at both $r_{ij} = R_s$ and $r_{ij} = R_c$; and so that the potential and its first two derivatives are monotonic for $R_s < r_{ij} < R_c$, and go to zero as $r_{ij} \to R_c$. These choices depend on the Ewald parameter $\alpha$ that occurs in both the real and reciprocal space contributions to the potential energy. For all $L$, we choose $\alpha = 2.5\,\mathrm{nm}^{-1}$ to ensure sufficient convergence of the potential energy in the reciprocal space summation for the densities studied. The value $R_c = 1$ nm where the switching function reaches zero is chosen to include third Si-Si neighbor interactions at most densities studied.

The real space contribution to $\Phi_{BKS}$, denoted here as $\phi$, is therefore a piece-wise defined function of the form,

$$\begin{aligned}
\phi(r_{ij} \le R_s) &= \frac{q_\mu q_\nu}{4\pi\varepsilon}\frac{\mathrm{erfc}(\alpha r_{ij})}{r_{ij}} \\
&+ A_{\mu\nu}e^{-B_{\mu\nu}r_{ij}} + \frac{C_{\mu\nu}}{r_{ij}^6} \\
&+ 4\epsilon_{\mu\nu}\left[\left(\frac{\sigma_{\mu\nu}}{r_{ij}}\right)^{30} - \left(\frac{\sigma_{\mu\nu}}{r_{ij}}\right)^{6}\right] \quad (3) \\
\phi(R_s < r_{ij} < R_c) &= D_{\mu\nu}(r_{ij} - R_s)^5 \\
&+ E_{\mu\nu}(r_{ij} - R_s)^4 \\
&+ F_{\mu\nu}(r_{ij} - R_s)^3 \quad (4) \\
\phi(r_{ij} \ge R_c) &= 0 \quad (5)
\end{aligned}$$

where erfc(x) is the complementary error function and $\varepsilon$ is the permittivity constant. The parameters are given in Table I.

Note that the above modifications have the consequence that the average potential energy $U$ and pressure $P$ obtained using $\Phi_{BKS}$ differ from those obtained using the standard BKS potential. We find that the differences are approximately independent of $T$ along isochores. At $T = 4000$ K and $\rho = 2.3072$ g/cm$^3$, we find that $\Phi_{BKS}$ gives a $P$ value 0.25 GPa greater than the standard BKS potential, and $U$ is 2.5 kJ/mol higher. At the same $T$ and $\rho = 3.8995$ g/cm$^3$, the respective differences are 0.9 GPa and 4.4 kJ/mol higher. These are not large differences on the scale of our measurements, and the qualitative behavior of the system is, as shown below, consistent with that found in other studies based on the BKS model.

For the free energy calculation to be described below, we also perform MD simulations using a binary Lennard-Jones (LJ) potential, in which two atomic species (also labeled "Si" and "O") occur in the same 1 : 2 proportion as in $SiO_2$. The LJ pair potential is of the form

$$\Phi_{LJ} = 4g_{\mu\nu}\left[\left(\frac{s_{\mu\nu}}{r_{ij}}\right)^{12} - \left(\frac{s_{\mu\nu}}{r_{ij}}\right)^{6}\right] - \Phi_{\mu\nu}^{\mathrm{shift}} \quad (6)$$

The pair potential is cut off at $r_{ij} = 2.5s_{\mu\nu}$ and $\Phi_{\mu\nu}^{\mathrm{shift}}$ is determined so that $\Phi_{LJ}(r_{ij} = 2.5s_{\mu\nu}) = 0$. These potential parameters are given in Table I.

In order to obtain equilibrium properties we use the following procedure. We equilibrate the liquid using velocity rescaling for a time $\tau$ long enough to allow Si atoms to diffuse an average of 0.2 nm, after significant relaxation of $P$ and $U$ have disappeared from the system history. The interval of velocity rescaling varies from 10 to 1000 time steps depending on $T$. The time step for all runs is 1 fs, except for $T = 7000$ K, where the time step is 0.5 fs. Velocity scaling is then turned off and the system is evolved in a constant $(N, V, E)$ ensemble for at least $10\tau$. ($E$ is the total energy.) Using this approach, there is no appreciable drift in $E$ during the constant $(N, V, E)$ phase, over which we calculate equilibrium quantities.

For the lowest $T$ where relaxation is slowest we modify this procedure to improve our sampling of phase space: we conduct up to five independent runs, with the constant $(N, V, E)$ phase of each run lasting at least $2\tau$. The reported properties (including $T$) are averages over both time and over the independent runs. Thus averages for low $T$ state points are also calculated over a total of $10\tau$, while at the same time the danger of an undetected trapping in an out-of-equilibrium state is reduced through comparison of the independent runs.

The densities of the isochores simulated are given in Table II, while the state points studied are shown in Fig. 1. Note that we have studied the isochore at density 2.3566 g/cm$^3$ in order to compare with previously published work [3]. The simulations along this isochore are those that involve only 999 atoms; all others model 1332 atoms.

## III. CONFIGURATIONAL ENTROPY CALCULATION

In this section we calculate $S_c$ from knowledge of $e_{IS}$ and the vibrational properties of the basins of the PES. Similar calculations have been carried out for water [20], binary LJ mixtures [21] and orthoterphenyl [9].

We begin by writing the Helmholtz free energy $F$ of the liquid along an isochore as [18],

$$F = e_{IS}(T) - TS_c(e_{IS}(T)) + f_{vib}(T, e_{IS}(T)). \quad (7)$$

| $\mu$-$\nu$ | Si-Si | Si-O | O-O |
|---|---|---|---|
| standard BKS parameters | | | |
| $A_{\mu\nu}$ (J $\times 10^{-16}$) | 0 | 28.845422 | 2.2250768 |
| $B_{\mu\nu}$ (nm$^{-1}$) | 0 | 48.7318 | 27.6 |
| $C_{\mu\nu}$ (J nm$^6$ $\times 10^{-23}$ ) | 0 | -2.1395327 | -2.8038308 |
| $\Phi_{BKS}$: short range parameters | | | |
| $\epsilon_{\mu\nu}$ (J $\times 10^{-22}$) | 0 | 4.963460 | 1.6839685 |
| $\sigma_{\mu\nu}$ (nm) | 0 | 0.1313635 | 0.1779239 |
| $\Phi_{BKS}$: switching function parameters | | | |
| $D_{\mu\nu}$ (J/nm$^5$ $\times 10^{-19}$) | -235.3529 | 122.0161 | -53.16278 |
| $E_{\mu\nu}$ (J/nm$^4$ $\times 10^{-19}$) | -117.7993 | 61.33742 | -26.25876 |
| $F_{\mu\nu}$ (J/nm$^3$ $\times 10^{-19}$) | -23.83785 | 12.33446 | -5.415203 |
| $\Phi_{LJ}$ parameters | | | |
| $g_{\mu\nu}$ (kJ/mol) | 23.0 | 32.0 | 23.0 |
| $s_{\mu\nu}$ (nm) | 0.33 | 0.16 | 0.28 |

TABLE I: Potential parameters used in this work for both $\Phi_{BKS}$ and $\Phi_{LJ}$. Also required to specify $\Phi_{BKS}$ are: $\alpha$ = 2.5 nm$^{-1}$, $R_s$ = 0.77476 nm, $R_c$ = 1 nm, $q_{\rm Si}$ = 2.4$e$ and $q_{\rm O}$ = 1.2$e$, where $e$ is the charge of an electron.

| Label | $V$ (cm$^3$/mol) | $V$ (cm$^3$/g) | $\rho$ (g/cm$^3$) | L (nm) |
|---|---|---|---|---|
| A | 5.1359 | 0.256443 | 3.8995 | 2.2479818 |
| B | 5.6423 | 0.281722 | 3.5496 | 2.3195561 |
| C | 6.1486 | 0.307012 | 3.2572 | 2.3869665 |
| D | 6.6550 | 0.332292 | 3.0094 | 2.4507704 |
| E | 7.1614 | 0.357577 | 2.7966 | 2.5114146 |
| F | 7.6677 | 0.382863 | 2.6119 | 2.5692635 |
| G | 8.1741 | 0.408147 | 2.4501 | 2.6246184 |
| H | 8.4984 | 0.424340 | 2.3566 | 2.4157510 |
| I | 8.6804 | 0.433426 | 2.3072 | 2.6777320 |

TABLE II: Isochore volumes, densities, and simulation box sizes studied in this work. All runs model 1332 particles, except for isochore H, where we model 999 particles. The reference volume $V_0$ corresponds to isochore I.

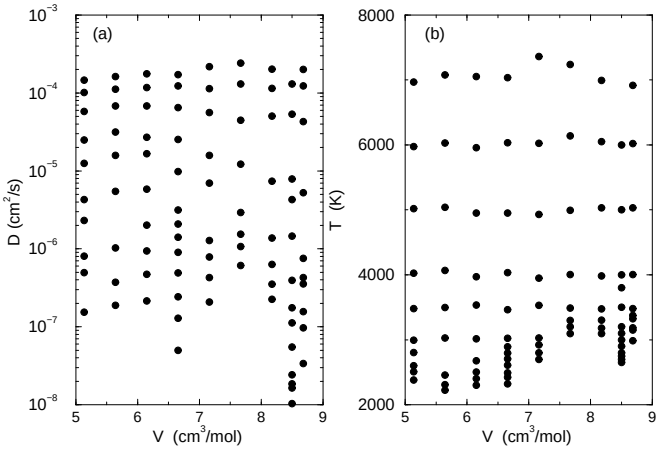


FIG. 1: State points simulated in the (a) $V$-$D$ and (b) $V$-$T$ planes. All points give results for equilibrated liquids.

This expression separates $F$ into two contributions: one stemming from the fact that the liquid samples different basins of the PES, and one arising from the properties of the basins themselves. $S_c$ is the entropy contribution resulting from basin degeneracy, i.e. it counts the number of basins associated with an inherent structure energy $e_{IS}$ [18, 21]. The vibrational part of the free energy $f_{vib}$ arises from the free energy of the basins. We note that the basin properties may change with $e_{IS}$, e.g., the vibrational density of states of a basin associated with low $e_{IS}$ may differ from that of one with high $e_{IS}$. In equilibrium, $F$ is minimized with respect to $e_{IS}$ and we obtain

$$\frac{\partial F}{\partial e_{IS}} = 0 = 1 - T\frac{\partial S_c}{\partial e_{IS}} + \frac{\partial f_{vib}}{\partial e_{IS}}. \tag{8}$$

We will provide evidence below that the vibrational properties of the basins do not change substantially from one $IS$ to another. In this case $\partial f_{vib}/\partial e_{IS} = 0$, and we may write,

$$S_c(T) = S_c(T_0) + \int_{T_0}^{T} \frac{1}{T'}\frac{\partial e_{IS}}{\partial T'}dT'. \tag{9}$$

$S_c(T_0)$ is the configurational entropy at a reference $T = T_0$.

Eq. 9 shows that the behavior of $S_c(T)$ is controlled by $e_{IS}(T)$. The work of Sastry [21] and others [18, 24] has shown that for fragile liquids, $e_{IS}$ decreases, and is negatively curved, as $T$ decreases. In accordance with Eq. 9, $S_c$ for fragile liquids also decreases, and is negatively curved, as $T$ decreases. If liquid silica is fragile at high $T$, and then crosses over to strong behavior at lower $T$, we expect that on cooling, both $e_{IS}$ and $S_c$ will initially behave as in a fragile liquid. However, from Eq. 1, strong behavior implies that $S_c$ (and hence $e_{IS}$) is constant with respect to $T$. Therefore, if the liquid passes from fragile to strong behavior as $T$ decreases, the implication is that $e_{IS}(T)$ will decrease with $T$ at high $T$, and then pass through a point of inflection, consistent with the approach to a constant at low $T$.

To obtain $S_c(T_0)$ we write,

$$S_c(T_0) = S(T_0) - S_{vib}(T_0), \tag{10}$$

where $S(T_0)$ is the total liquid entropy and $S_{vib}(T_0)$ is the entropy contribution arising from the vibrational properties of basins in the PES. The vibrational part has both a harmonic and an anharmonic contribution, which we calculate separately:

$$S_{vib}(T) = S_{harm}(T) + S_{anh}(T), \tag{11}$$

where [36]

$$S_{harm} = \frac{R}{N}\sum_{i=1}^{3N-3}\left(1 - \ln\frac{\hbar\omega_i}{kT}\right), \tag{12}$$

and

$$S_{anh} = \int_0^T \frac{1}{T'}\frac{\partial E_{anh}}{\partial T'}dT'. \tag{13}$$

Here $S_{harm}$ is the entropy in the harmonic approximation of the IS's obtained at a given $T$. The set $\{\omega_i\}$ describes the vibrational density of states of the IS's (details below), $\hbar$ is Planck's constant over $2\pi$, $R$ is the gas constant, and $k$ is Boltzmann's constant. $E_{anh}$ is given by

$$E_{anh}(T) = E(T) - E_{harm}(T) - e_{IS}(T), \qquad (14)$$

where $E_{harm}$ is the harmonic contribution to the energy, given by $E_{harm} = 3RT(N-1)/N$.

To obtain $e_{IS}$ we select 100 equilibrated liquid configurations over the course of the MD run, perform a conjugate gradient minimization [37] of $\mathcal{U}$, and then average the results. As a stopping criterion for the conjugate gradient minimizations, we specify a relative tolerance of $10^{-8}$ along line minimizations and a relative tolerance of $10^{-15}$ between line minimizations. In the case of isochore H our runs are the longest, and so we average over 1000 configurations.

In order to evaluate $S_c$ and $S_{anh}$ (using Eqs. 9 and 13 respectively) we first fit average values of $e_{IS}$ and $E_{anh}$ to polynomials in $T$, and then evaluate the required integrals analytically. The $E_{anh}$ fit is constrained so that at $T = 0$, the value of $E_{anh}$ and its first derivative are zero. This is consistent with $E_{anh}$ being a correction to the harmonic approximation.

It is important to recognize that the expression for $S_{anh}$ in Eq. 13, and hence the estimation of $S_c$ via Eqs. 9-14, is valid only under the assumption that the basin anharmonicity does not change from basin to basin. To understand this, consider the expression for $E_{anh}$ in Eq. 14, from which $S_{anh}$ is calculated. The terms contributing to $E_{anh}$ are evaluated from equilibrium liquid properties. Yet, an implication of Eq. 14 is that an IS obtained from a liquid at (e.g.) 4000 K, when heated itself to 4000 K, will give a value of $E_{anh}$ equal to that obtained from equilibrium configurations at 4000 K. However, an IS obtained from a liquid at 3000 K, when heated to 4000 K will not necessarily yield the value of $E_{anh}$ found from equilibrium configurations at 4000 K, because IS's obtained from different $T$ may be in basins of different shape, and hence different anharmonicity. If the basin shape does change with $e_{IS}$, then $S_c$ in Eq. 9 will be influenced by an additional contribution. Moreover, Eq. 14 would be invalid and $E_{anh}$ would have to be obtained in a different way, possibly by a careful heating of individual basins obtained from the equilibrium liquid at different $T$. Such heating experiments must be performed with care, as the system must not diffuse out of the basin if accurate results are to be obtained.

To test if basins associated with different $T$ have different shapes, we carry out runs in which IS's from different $T$ and $V$ are rapidly heated. We find that $E_{anh}$ is the same for all basins belonging to the same isochore up to high $T$ (Fig. 2).

Based on the relations justified above, we can evaluate $E_{anh}(T)$ and $S_{anh}(T)$ from a knowledge of $e_{IS}(T)$. We can also evaluate $S_c(T)$, up to a constant, from $e_{IS}(T)$.

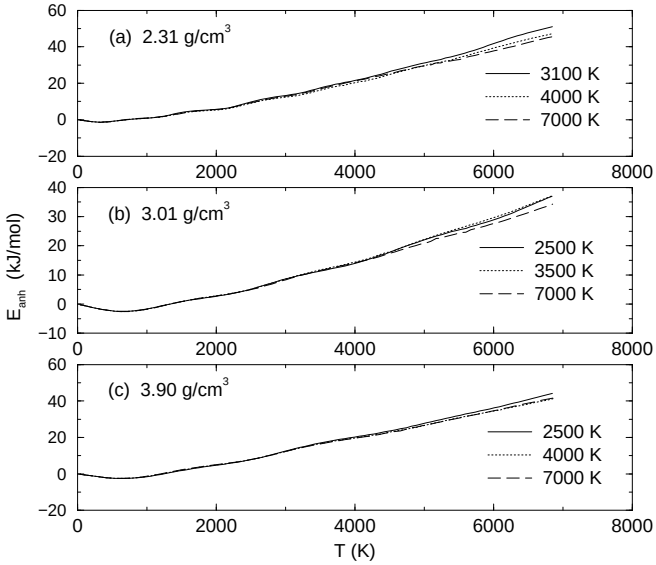


FIG. 2: Test of $T$-dependence of basin shape. IS's from three $T$, and for three isochores, are rapidly heated in order to confine the sampling to a single basin. Using velocity scaling, $T$ is increased from 0 K to 7000 K over 100 fs. Each curve is an average over 10 runs. The curves for the same isochore are approximately the same, indicating that the anharmonic contributions to the vibrational energy can be assumed, for the present purposes, to be the same for each basin

To complete an evaluation of $S_c(T)$, we need to estimate both $S_{harm}(T)$ and $S(T_0)$ for each isochore to be studied, as described in the following two subsections.

### A. Harmonic Entropy of Inherent Structures

We define $S_{harm}$ of the liquid as the average harmonic entropy of IS's sampled from the liquid. When a liquid configuration is quenched to its corresponding IS, it becomes a mechanically stable solid, and is to a first approximation, harmonic. To calculate the entropy of an IS in the harmonic approximation, we require its vibrational density of states. As each IS is an atomic configuration at a local minimum of the PES, we expand the expression for $\mathcal{U}$ about the local minimum:

$$\mathcal{U} = e_{IS} + \sum_{i=1}^{3N}\sum_{j=1}^{3N} q_i \left.\frac{\partial^2 \mathcal{U}}{\partial q_i \partial q_j}\right|_{q=q_0} q_j. \qquad (15)$$

Here, the set $\{q_i\}$ specifies the 3N atomic coordinates, and the notation "$q = q_0$" denotes that the second derivatives are evaluated at the minimum energy configuration. We then define a Hessian matrix,

$$H_{ij} = \frac{1}{\sqrt{m_i m_j}} \left.\frac{\partial^2 \mathcal{U}}{\partial q_i \partial q_j}\right|_{q=q_0}, \qquad (16)$$

where $m_i$ is the mass of the atom associated with coordinate $q_i$. Since the system is at a minimum, $H_{ij}$ has

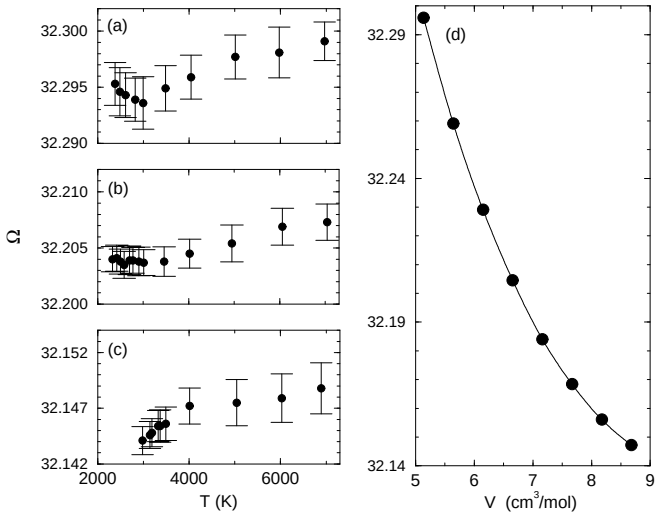


FIG. 3: Ω as a function of $T$ for (a) isochore A, (b) isochore D, and (c) isochore I. Also shown is the standard deviation about the mean value based on 100 samples. We note that a difference in Ω of 0.01 yields a change in entropy of 0.24 J/mol K. For the purpose of this work, we therefore consider Ω to be constant along isochores. (d) $\Omega(T = 4000\,\mathrm{K})$ as a function of $V$; this is the value of Ω used in our calculations.

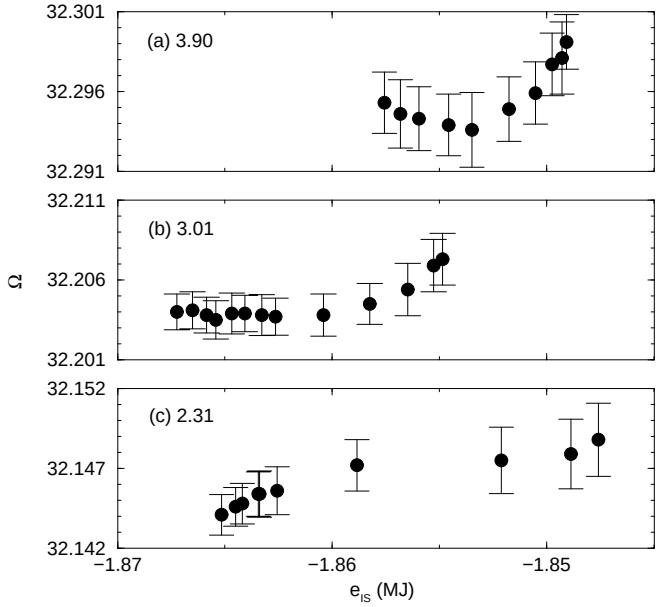


FIG. 4: Ω as a function of $e_{IS}$ for (a) isochore A, (b) isochore D, and (c) isochore I. The error bars represent the standard deviation about the mean value based on 100 samples.

eigenvalues $\{h_i\}$ all greater than zero, except for three zero eigenvalues which account for the three independent translations of the entire system. These three eigenvalues are excluded in calculating the harmonic entropy. The $w_i$ appearing in Eq. 12 are defined as $w_i = \sqrt{h_i}$. We note that a particular Hessian matrix corresponds to an IS obtained from a liquid configuration at a certain $T$. It is this $T$ that we use in Eq. 12.

We find, perhaps surprisingly, that the spectrum of $w_i$ does not change appreciably with $T$ along isochores. We plot in Fig. 3 the quantity,

$$\Omega(T) = \left\langle \frac{1}{3N-3} \sum_{i=1}^{3N-3} \ln w_i \right\rangle \qquad (17)$$

to show that the contribution to $S_c$ from changes in Ω as $T$, and hence $e_{IS}$, is varied is negligible. This quantity is part of the expression for $S_{harm}(T)$. It captures the average quadratic shape of a basin and hence determines any dependence of $S_{harm}$ on $e_{IS}$. The plot shows Ω not to vary appreciably with $T$, and we conclude that there is no contribution to $S_c$ from $f_{vib}$, at least not from the harmonic portion.

To confirm this approximation, we show in Fig. 4 the variation of Ω with $e_{IS}$. We find that the change in Ω can be as large as $\Delta\Omega \simeq 0.006$ for variations of $e_{IS}$ as small as $\Delta e_{IS} \simeq 5$ kJ. This gives a contribution to $\partial f_{vib}/\partial e_{IS}$, the last term in Eq. 8, of at most $RT\Delta\Omega/\Delta e_{IS} \simeq 0.04$. This supports our assumption that $\partial f_{vib}/\partial e_{IS} = 0$.

### B. Liquid Entropy

To exploit the AG relation, we require the absolute value of $S_c$, not just changes in $S_c$ from one state point to another. To evaluate $S_c(T_0)$ in Eq. 10 requires $S(T_0)$, the absolute entropy of the BKS liquid, which we calculate via thermodynamic integration starting from a system for which the entropy is known exactly.

As our starting point we use the analytic result for the entropy of an ideal gas composed of two species of particles, each with its own mass [36],

$$\begin{aligned} S_{IG} &= N_{Si}k\left\{\ln\left[\frac{V}{N_{Si}}\left(\frac{2\pi m_{Si}kT}{h^2}\right)^{\frac{3}{2}}\right]+\frac{5}{2}\right\} \\ &+ N_O k\left\{\ln\left[\frac{V}{N_O}\left(\frac{2\pi m_O kT}{h^2}\right)^{\frac{3}{2}}\right]+\frac{5}{2}\right\} \\ &- k\ln\left(2\pi\sqrt{N_{Si}N_O}\right). \end{aligned} \qquad (18)$$

For simplicity, we continue to label the two species as "Si" and "O". Note that $h$ is Planck's constant, and that the Stirling approximation has been employed in the derivation of this result, i.e. $\ln N! \approx N\ln N - N + \ln(2\pi N)^{1/2}$.

For the purpose of thermodynamic integration, we approximate this ideal gas with a dilute binary LJ system in which the stoichiometry of the species is the same as that of Si and O in our silica simulations, i.e. $N_{Si} = 444$ and $N_O = 888$.

We equilibrate the LJ system at a reference $T = T_0 = 4000$ K over a range of $V$ from a reference $V = V_0 = 8.6804\,\mathrm{cm}^3/\mathrm{mol}$ to $V = 173610\,\mathrm{cm}^3/\mathrm{mol}$. Denoting the

reference state point at $(T_0, V_0)$ as "$C$", the entropy of the LJ liquid $S_{LJ}$ at $C$ can be written,

$$S_{LJ}(C) = S_{IG}(C) + \frac{U_{LJ}(C)}{T} - \frac{1}{T}\int_{V_0}^{\infty} P_{LJ}^{ex} dV. \quad (19)$$

$S_{IG}(C) = 117.236$J/mol K is calculated from Eq. 18. From simulations we obtain $U_{LJ}(C) = -134099 \pm 50$ J/mol, the potential energy of the LJ system at $C$. $P_{LJ}^{ex} = P_{LJ} - NkT/V$ is the excess pressure of the LJ system, which we evaluate for many $V$ at $T_0$ (Fig. 5).

In order to evaluate the integral in Eq. 19, we seek a function to fit to our $P_{LJ}^{ex}$ data that we can integrate analytically. A natural choice is the virial expansion for $P_{LJ}^{ex}$, a power series in $1/V$. At sufficiently large $V$, the $V$ dependence of $P_{LJ}^{ex}$ will be well approximated by the leading term in the virial expansion,

$$P_{LJ}^{ex} \simeq \frac{b_2 kTN^2}{V^2}, \quad (20)$$

where for our binary system,

$$b_2 = 1/9\, b_2^{SiSi} + 4/9\, b_2^{SiO} + 4/9\, b_2^{OO}, \quad (21)$$

and the coefficients $b_2^{\mu\nu}$ are defined by,

$$b_2^{\mu\nu} = -4\pi \int_0^{\infty} r^2 \big(e^{-\Phi_{LJ}(\mu,\nu,r)/kT} - 1\big) dr. \quad (22)$$

We calculate $b_2$ numerically for the LJ system and find $b_2 = -0.0337\,\mathrm{nm}^3$. As shown in Fig. 5, we have simulated the LJ fluid to large enough $V$ so that $P_{LJ}^{ex}$ conforms to Eq. 20. To integrate $P_{LJ}^{ex}$ over $(V_0, \infty)$, we fit the data to

$$P_{LJ}^{ex} = \frac{b_2 kTN^2}{V^2} + \sum_{n=3}^{M} \frac{a_n}{V^n}, \quad (23)$$

and use this form to evaluate the integral in Eq. 19. We evaluate the integral using three different fits with $M =$ 6, 7 and 8 in order to obtain an error estimate for the integral. We estimate the value of the integral to be $-1268 \pm 700$ J/mol, and thus find $S_{LJ}(C) = 84.028 \pm 0.175$ J/mol K.

To obtain $S(C)$ from $S_{LJ}(C)$ we perform a generalized thermodynamic integration [38], in which a parameter $\lambda$ is used to create a continuous path between the LJ system at $C$ and the BKS system at $C$. To this end, we conduct MD simulations of a system of particles interacting via a pair potential $\Phi$ such that,

$$\Phi(\lambda) = \lambda \Phi_{BKS} + (1-\lambda)\Phi_{LJ}. \quad (24)$$

When $\lambda = 0$, the system corresponds to the LJ fluid, and when $\lambda = 1$, the system corresponds to the BKS potential. For arbitrary $\lambda$, the instantaneous potential energy is given by,

$$\mathcal{U}_\lambda = \lambda \mathcal{U}_{BKS} + (1-\lambda)\mathcal{U}_{LJ}, \quad (25)$$

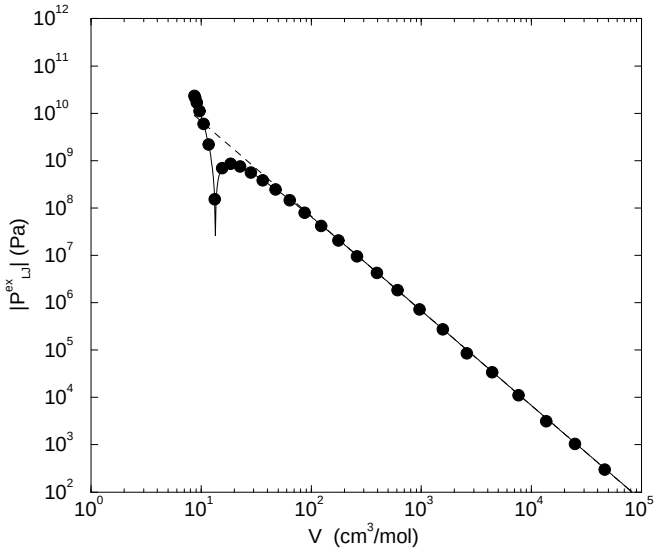


FIG. 5: Isotherm of $|P_{LJ}^{ex}|$ for the LJ fluid at $T = 4000$ K. The solid line is the fit to Eq. 23 with $M = 8$. The dashed line is the curve given by Eq. 20. The data are shown on a log-log plot to simplify the comparison of the data to Eq. 20 at large $V$. The cusp near $V = 10\,\mathrm{cm}^3$/mol is due to the fact that $P_{LJ}^{ex}$ changes sign.

where $\mathcal{U}_{BKS}$ ($\mathcal{U}_{LJ}$) is the instantaneous potential energy of the system evaluated using only the $\Phi_{BKS}$ ($\Phi_{LJ}$) pair potential. The Helmholtz free energy difference $\Delta F = F_{BKS} - F_{LJ}$ between the BKS and LJ systems at $C$ is given by,

$$\begin{aligned} \Delta F(C) &= \int_0^1 \left\langle \frac{\partial \mathcal{U}_\lambda}{\partial \lambda} \right\rangle_\lambda d\lambda \\ &= \int_0^1 \langle \mathcal{U}_{BKS} - \mathcal{U}_{LJ} \rangle d\lambda. \end{aligned} \quad (26)$$

We evaluate the above integral by simulating the system governed by Eq. 24 at several values of $\lambda$ and using a cubic spline to interpolate between points. The integrand is shown in Fig. 6, from which we obtain $\Delta F(C) = -1635990 \pm 50$ J via numerical integration.

From our BKS simulations we find $U(C) = -1802257 \pm 100$ J/mol, from which we evaluate $\Delta U(C) = U(C) - U_{LJ}(C)$. Using $S(C) = S_{LJ}(C) + [\Delta U(C) - \Delta F(C)]/T$, we find for the BKS liquid $S(C) = S(T_0, V_0) = 75.986 \pm 0.177$ J/mol K.

To obtain values of $S$ at $T_0$ for $V$ different from $V_0$, we carry out a thermodynamic integration of $P$ along an isotherm of the BKS liquid, using,

$$\begin{aligned} S(V, T_0) &= S(C) + \frac{1}{T}\big[U(V, T_0) - U(C)\big] \\ &+ \frac{1}{T}\int_{V_0}^{V} P(V')dV'. \end{aligned} \quad (27)$$

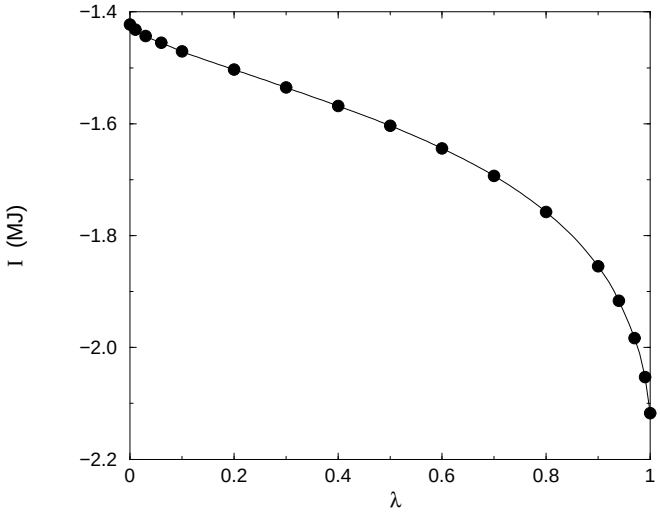


FIG. 6: Plot of the integrand $I = \langle \mathcal{U}_{BKS} - \mathcal{U}_{LJ} \rangle$, in Eq.26. The solid line is a cubic spline fit to the data.

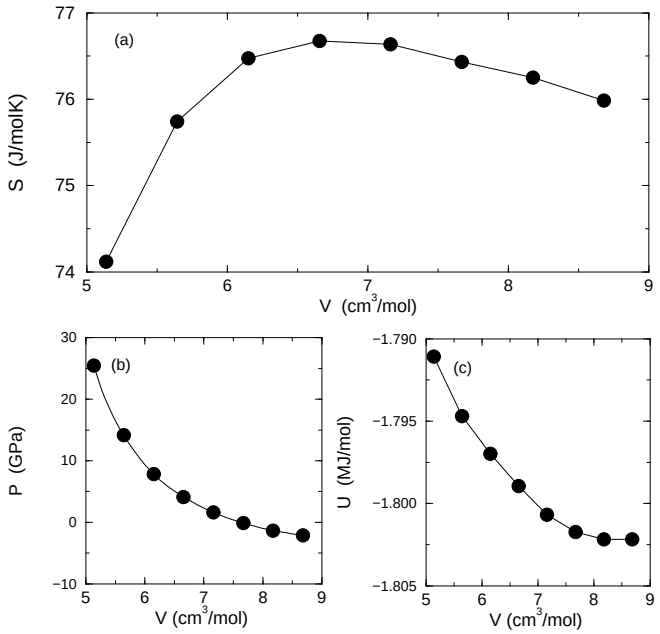


FIG. 7: Thermodynamic properties of liquid BKS silica along the $T_0 = 4000$ K isotherm: (a) $S$, (b) $P$, and (c) $U$.

To evaluate the above integral, we find $P$ for various $V$ at $T_0$ and fit the data with a cubic spline. This spline fit is then used to generate data for a numerical evaluation of the integral. We thus have $S(V, T_0)$, the absolute entropy of the BKS liquid at all $V$ studied, at $T_0 = 4000$ K (Fig. 7).

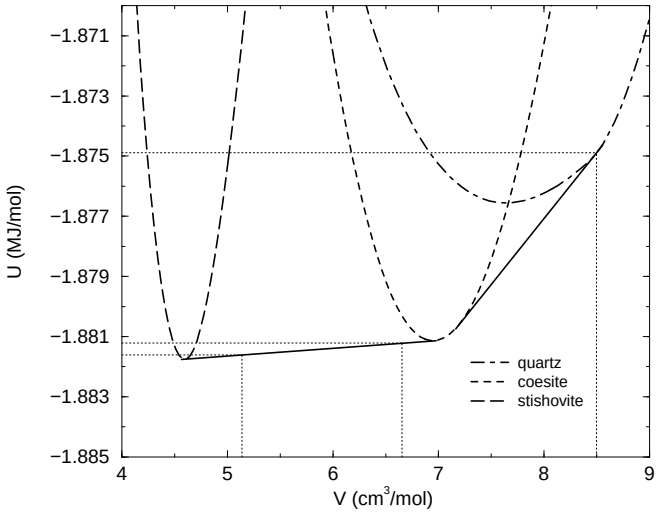


FIG. 8: $U(V, T = 0)$ for quartz, coesite and stishovite. Solid lines are common tangent constructions used to find the system ground state energy for specific values of $V$ (as indicated by dotted lines).

### C. Crystalline Ground States

As discussed in the next section, we also find it useful to calculate the $T = 0$ crystalline ground state energy $U(0)$ of the BKS system, for comparison with the IS energies obtained from the quenched liquid configurations.

To this end, we study three crystalline structures of silica important in the $V$ range under consideration, namely quartz, coesite and stishovite [39, 40, 41]. We evaluate the $T = 0$ energy curves for these crystals as modeled by the $\Phi_{BKS}$ pair potential. Starting from the previously determined crystal structures, we optimize $U(0)$ of the model system through an iterative procedure where we alternately minimize $U(0)$ as a function of the particle coordinates in a simulation cell of fixed geometry, using a conjugate-gradient procedure; and then optimize the cell geometry with a simplex method [37]. During the cell geometry optimization, we constrain $V$ to be fixed, but otherwise allow the shape to change. This is done to remove anisotropic stress within the crystal while preserving $V$. Once the crystal structure has been optimized for a particular $V$, we incrementally change $V$ and repeat the optimization. The results for the three crystals are shown in Fig. 8. At fixed $V$, the thermodynamic ground state may be a single crystal phase, or a coexisting mixture of two crystalline phases. To obtain the ground state energy in the case of a mixture, we employ the "common tangent construction," as shown in Fig. 8.

## IV. RESULTS AND DISCUSSION

The calculations described above yield a complete thermodynamic description of the BKS model of liquid silica,

including the absolute free energy of the model, and the absolute configurational entropy, over a wide range of $V$-$T$ conditions. Combined with dynamical data, in the form of the diffusion coefficient $D$, a number of conclusions may be drawn, as described below. Note in the following that by $D$ we mean the diffusion coefficient of the Si atoms, evaluated from the particle mean squared displacement in equilibrium. For comparison we also show some results for the diffusion coefficient of the O atoms, $D_O$. In general, the qualitative results are independent of the choice of atomic species.

### A. Signature of fragile-to-strong crossover in the potential energy landscape

Our results for $D$ are shown in Figs. 9(a) and 10(a). These plots take the form of Arrhenius plots of $D$ and $D/T$ respectively, the latter quantity being preferred in some works as a measure of particle mobility in liquids. As first observed in Ref. [3], the FSC of the BKS model can be seen in our simulations at low $\rho$, which correspond to the value of $\rho$ for real silica at ambient $P$; isochores are curved on an Arrhenius plot at high $T$, but becomes straighter at the lowest $T$.

We compare the behavior of $D$ and $D_O$ in Fig. 11. We find that the ratio of $D_O/D$ varies between 1 and 3, but that the $T$ dependence of $D_O$ is qualitatively the same as that of $D$.

Our results for $e_{IS}$ and $S_c$ are shown in Figs. 12, 13 and 14. Note that our estimates for $S_c$ have changed somewhat, compared to the values published in Ref. [31], due to improved averaging using more data, as well as refinements in our analysis. However, the qualitative results of Ref. [31] remain in agreement with those presented here.

Consistent with the predictions made in Section III, we find that for the low $\rho$ isochores, where a FSC is observed, we also observe a point of inflection in the $T$ dependence of both $e_{IS}$ and $S_c$. This inflection is what one would expect if the emergence of strong liquid behavior with decreasing $T$ is associated with the approach of $e_{IS}$ and $S_c$ to a constant at low $T$.

Ref. [21] showed that for a binary Lennard-Jones mixture at low $T$, $e_{IS}(T) \sim -\frac{1}{T}$. This $T$-dependence of $e_{IS}$, consistent with a Gaussian distribution of IS energies, has been observed in other models [9, 24]. Furthermore, the binary LJ system is a relatively fragile liquid, and in this regard, our results for silica at high $\rho$ are similar to those for binary LJ (inset, Fig. 12). This is consistent with the fact that at high $\rho$ the network structure of liquid silica is disrupted, giving behavior more like that of simpler liquids, such as the binary LJ system. We also find that the $T$-dependence of $S_c$ becomes more like that of a simple, fragile liquid (Fig. 14) as $\rho$ increases.

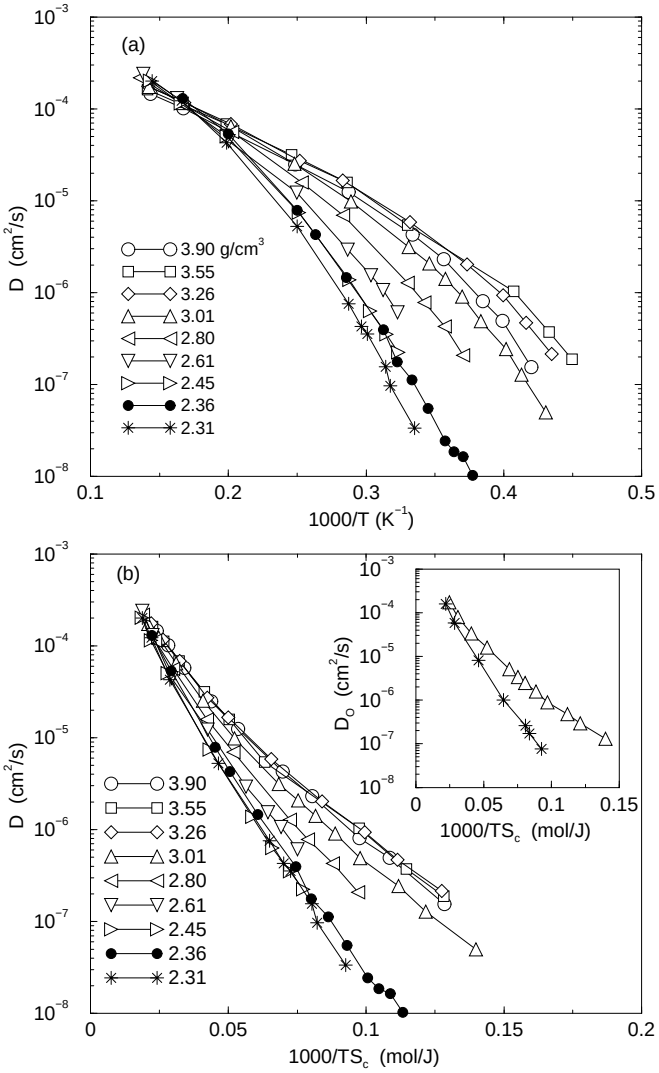


FIG. 9: (a) Isochores of $D$, the diffusion coefficient of Si atoms. (b) Test of the AG relation along isochores of $D$; the legend indicates $\rho$ in g/cm$^3$. If the data fall on a straight line, the AG relation is satisfied. For comparison, the inset shows $D_O$, the diffusion coefficient of O atoms, along the $\rho = 3.01$ (triangles) $\rho = 2.31$ g/cm$^3$ isochores (stars).

### B. Implications for the Kauzmann paradox

In Fig. 13, we compare the behavior of $e_{IS}$ to the $T = 0$ energy of the crystalline state of the system, as found from the data in Fig. 8. It is interesting to note how closely $e_{IS}$ approaches the crystal energy at low $\rho$, compared to the behavior at higher $\rho$. We do not expect $e_{IS}$, the energy of a disordered configuration obtained from the liquid at $T$, to ever be less than that of the $T = 0$ crystalline state of the system. The $T$-dependence of $e_{IS}$ at low $\rho$ is consistent with behavior that would respect this constraint as $T \to 0$. At higher $\rho$, $e_{IS}$ does not approach the crystal energy as closely as it does at lower $\rho$. The conditions that might induce an inflection in $e_{IS}$ are

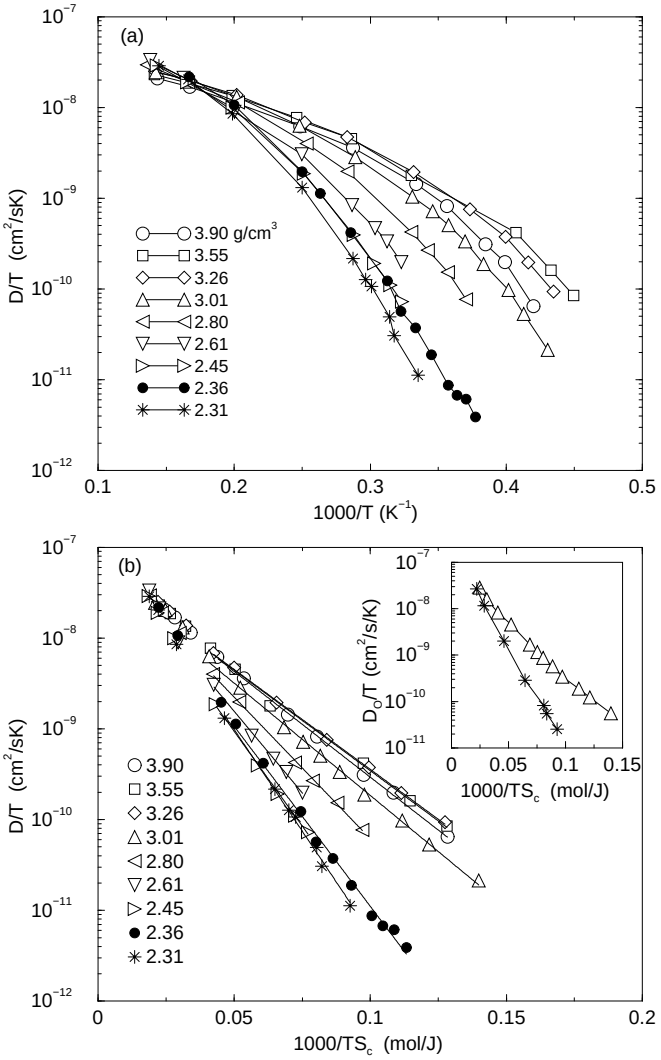


FIG. 10: (a) Isochores of $D/T$. (b) Test of the AG relation along isochores of $D/T$; the legend indicates $\rho$ in g/cm$^3$. For comparison, the inset shows $D_O$ along the $\rho = 3.01$ (triangles) $\rho = 2.31$ g/cm$^3$ isochores (stars). The lines in the main panel are fits of a straight line to the data, used to obtained the values of $A$ and $\mu_0$ shown in Fig. 15

.

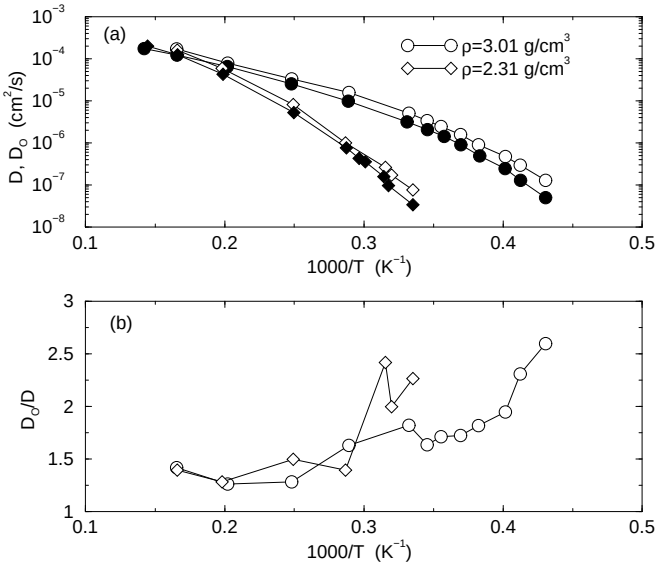


FIG. 11: (a) Arrhenius plot of $D_O$ (open symbols) and $D$ (filled symbols) along the $\rho = 3.01$ (circles) and $\rho = 2.31$ g/cm$^3$ (diamonds) isochores. (b) Ratio $D_O/D$ as a function of $1/T$ along the isochores shown in (a).

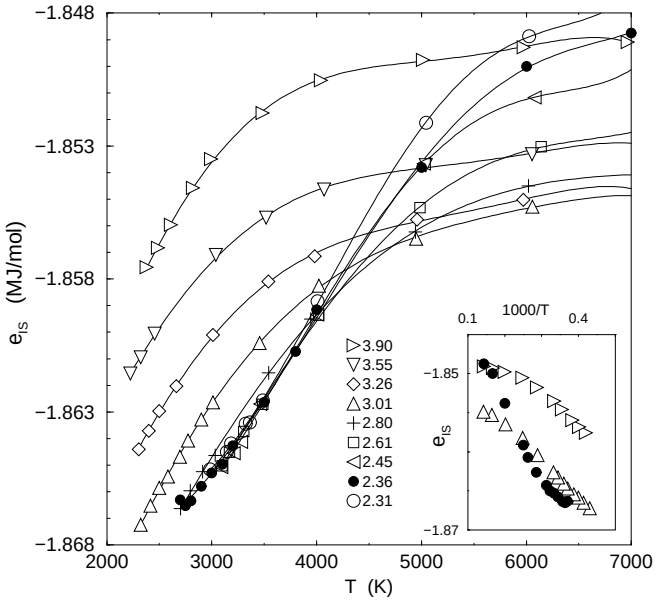


FIG. 12: $e_{IS}(T)$ along isochores. The lines are fits to each isochore of a fifth order polynomial in $T$ with no linear term (i.e. zero slope at $T = 0$); these are the polynomial curves we use to estimate the integral term in Eq. 9. The legend indicates $\rho$ in g/cm$^3$. The inset shows $e_{IS}$ versus $1/T$ for three isochores spanning the density range. The low density isochore shows a marked departure from the relation $e_{IS} \sim 1/T$ at low $T$. The symbols used in the inset correspond to the same $\rho$ as in the main panel.

therefore not realized in the $T$ range of our simulations.

The inflection in $e_{IS}$ is associated with an inflection in the $T$-dependence of $S_c$, also found at low-$\rho$ (Fig. 14). For real systems, the third law of thermodynamics requires that the lower bound for $S_c$ be zero. Although our system is purely classical, the same constraint applies, because the configurational entropy we calculate counts the number of basins explored by the liquid, which is necessarily one or greater. As pointed out by Kauzmann in 1948 [42], the entropy as $T$ decreases of many supercooled liquids initially decreases at a sufficiently high rate so as to suggest that the entropy might reach zero at finite $T$ (the so-called "entropy catastrophe"). That this purely thermodynamic event seems to be preempted by

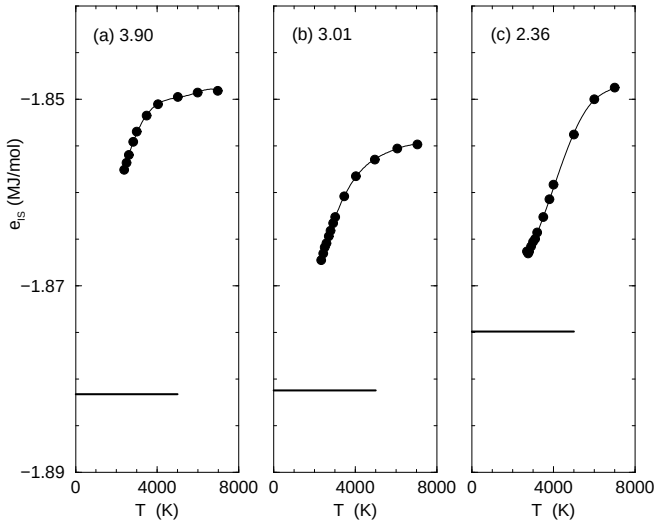


FIG. 13: Detail of isochoric $e_{IS}$ behavior for three $\rho$ spanning the range of our calculations. The thick horizontal lines show the value of the $T = 0$ crystal energies obtained from Fig. 8.

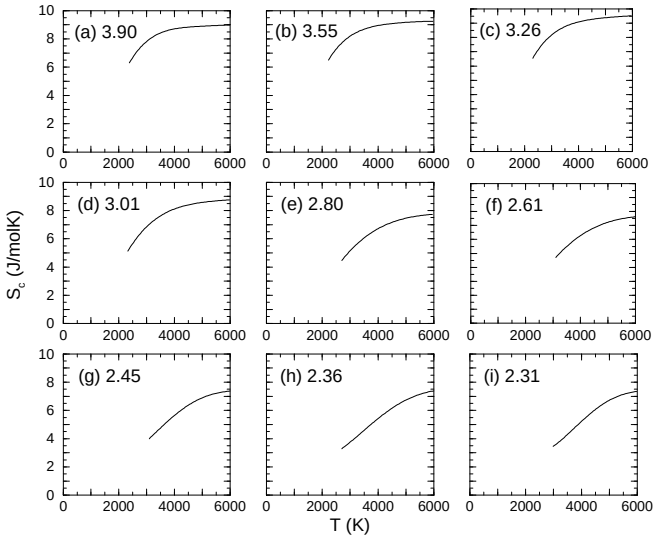


FIG. 14: $S_c$ along isochores; each panel is labeled by the density in g/cm$^3$. Each curve is obtained using Eq. 9, by integrating the fitted curves for $e_{IS}$ shown in Fig. 12.

the occurrence of a kinetic event, the glass transition, is the so-called "Kauzmann paradox." At low $\rho$ and high $T$, we find that $S_c$ behaves in similar fashion, decreasing rapidly as $T$ decreases. An extrapolation of the observed high $T$ behavior raises the possibility that $S_c$ might reach zero at finite $T$. However, the inflection observed in the lower part of our observed $T$ range establishes behavior that allows Kauzmann's "entropy catastrophe" to be avoided through a purely thermodynamic phenomenon.

It is therefore tempting to speculate that our observations may be transferable to other systems to which the Kauzmann paradox seems to apply. How $S_c > 0$ is maintained in deeply supercooled liquids can perhaps be understood in terms of the PES changes observed here. Moreover, the PES change we find in BKS silica is correlated to the fragile-to-strong dynamical crossover. Hence it is possible that the FSC and (the avoidance of) the Kauzmann paradox are fundamentally interrelated phenomena.

However, if the above speculations are confirmed, it is important to note the differences between silica and other supercooled liquids. The picture developed above implies that the $T$ range of the phenomenon by which silica avoids the Kauzmann paradox is above, and widely separated from, $T_g$ in silica. In other supercooled liquids, the glass transition may occur at $T$ above, and thus obscure, the PES changes found here. More work on these possibilities is clearly required.

### C. Test of the Adam-Gibbs relation

In order to draw the conclusions given above, we must also test that the liquid satisfies the AG relation. If $S_c$ does not control the behavior of $D$, then we will lack the basis required for making a connection between the behavior of the PES and the liquid dynamics.

We perform this test by plotting $\log(D)$ [Fig. 9(b)] and $\log(D/T)$ [Fig. 10(b)] against $\log(1/TS_c)$. The AG relation is obeyed by data that follows a straight line on such a plot. We find that the isochores of $D/T$ provide the best agreement with the AG relation. Note also that both high and low $\rho$ isochores, regardless of whether $S_c$ exhibits an inflection, obey the AG relation. Thus we see that regardless of dynamical regime (fragile or strong), and regardless of inflections in the $T$ dependence of $S_c$ or $e_{IS}$, the liquid behaves so as to satisfy the AG relation. This observation reinforces the positive tests of the AG prediction that have been documented in other work (see e.g. Ref. [9, 20, 21, 43]).

In Fig. 15 we present estimates of the constants $A$ and $\mu_0$ that appear in Eq. 1. These are obtained by fitting straight lines to the isochores in Fig. 10(b), omitting the three data points at the highest $T$, where deviations from the AG relation are expected.

### D. Entropy and Diffusion

In the case of simulated water [20], it was found that maxima of $S_c$ isotherms occur, within error, at the same $V$ as the maxima in isotherms of $D$. We show our results for the $V$ dependence of $D$, $S_c$ and $S$ in Fig. 16. At lower $T$, isotherms of $S_c$ and $D$ pass through a maximum at approximately the same $V$. However, as $T$ increases, the correlation of these maxima fades. This may be due in part because at higher $T$, our estimates of $S_c$ worsen, due to the larger role played by the anharmonic corrections. At the highest $T$, the trend is for isochores of $D$, $S_c$ and $S$ to become monotonic functions of $V$. An obser-

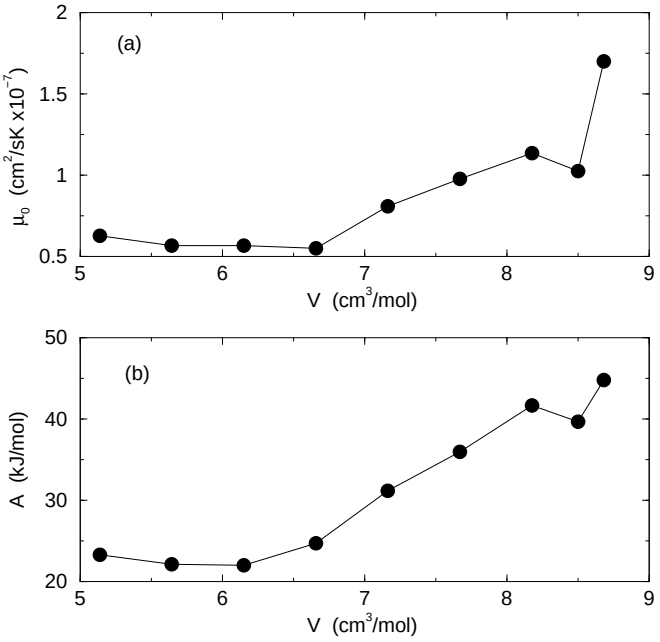


FIG. 15: Estimates of the parameters (a) $\mu_0$ and (b) $A$, that occur in Eq. 1. These estimates are based on the straight-line fits to the data shown in Fig. 10(b).

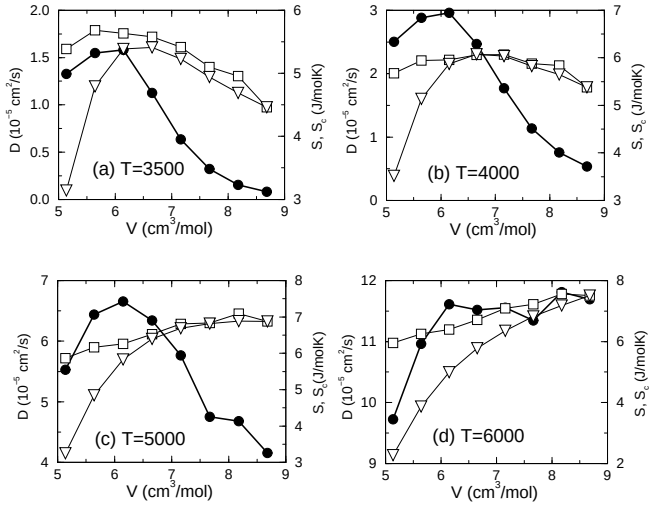


FIG. 16: Isotherms of the $V$ dependence of $D$ (filled circles), $S_c$ (squares) and $S$ (triangles) at various $T$. For plotting purposes, $S$ has been shifted down so that $S(V_0) = S_c(V_0)$. The shifts in $S$ for the various panels are (a) $-66.6042$ J/mol K, (b) $-70.6031$ J/mol K, (c) $-77.8919$ J/mol K, and (d) $-84.3673$ J/mol K.

vation that the $V$ dependence of entropy follows that of $D$ would be consistent with recent work examining the relationship between structural disorder and diffusivity in BKS silica [44].

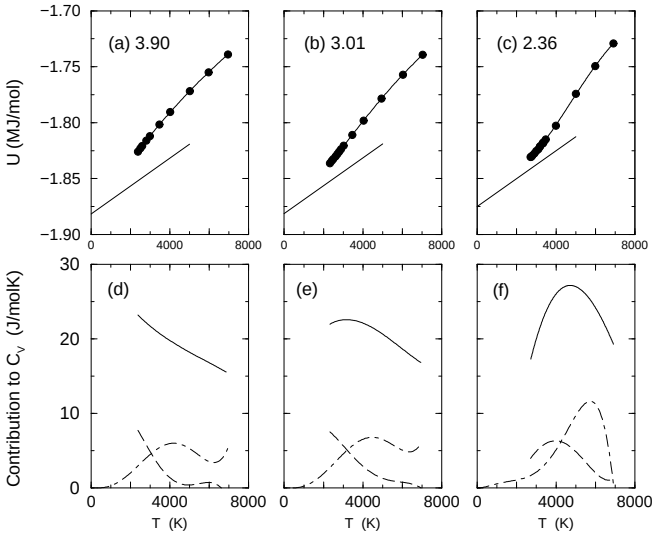


FIG. 17: Comparison of $U$ and the contributions to $C_V$. The top panels (a)-(c) show isochores of $U$ spanning the studied density range; also shown are estimates for $U$ of the crystalline state of the system in the harmonic approximation, derived from the $T = 0$ estimate of $U$ in Fig. 8 and extended to higher $T$ using a straight line of slope $3R/2$. The bottom panels (d)-(f) show the contributions to $C_V$. The solid line is $C_V - (3R/2)(N-1)/N$; the dot-dashed line is $C_V^{anh}$; and the dashed line is $C_V^{IS}$. Each curve is obtained by differentiating the function fitted to the data for the corresponding energy.

### E. Specific heat

In terms of the various contributions to $E = e_{IS} + E_{anh} + 3RT(N-1)/N$, we can write the constant volume specific heat $C_V$ as,

$$C_V = \left(\frac{\partial E}{\partial T}\right)_V = \left.\frac{\partial}{\partial T}\right|_V \left(e_{IS} + E_{anh} + \frac{3RT(N-1)}{N}\right). \quad (28)$$

So written, we can separately evaluate the contributions to $C_V$ from $e_{IS}$ and $E_{anh}$, which we denote $C_V^{IS}$ and $C_V^{anh}$ respectively (Fig. 17). At all $\rho$, $C_V^{anh}$ exhibits a maximum; at the lowest $\rho$ the inflection in the $T$ dependence of $e_{IS}$ means that $C_V^{IS}$ also passes through a maximum. Together, at low $\rho$, the strength of these two contributions becomes large enough to give a peak in the total value of $C_V$. This peak is therefore a thermal signature approximately demarcating the crossover from fragile to strong dynamical behavior. It would be interesting to explore if such signatures could be observed in high $T$ experiments on silica, or related systems [45].

### F. Relation to polyamorphism

Real amorphous solid silica displays "polyamorphism," the conversion under pressure of a low density form to a

high density form, that occurs in some ways as though it were a first-order phase transition. Computer simulations of BKS silica have provided evidence that this polyamorphic transition may correspond to a sub-$T_g$ remnant of a liquid-liquid phase transition occurring in the equilibrium liquid [46].

Having found that the same model, BKS silica, exhibits a thermodynamic anomaly, in the form of a $C_V$ peak associated with a FSC, it is natural to ask if this phenomenon is related in some way to polyamorphism. It is difficult at present to answer this question decisively, since the region of the proposed liquid-liquid instability in BKS silica has only been approximately located, and seems to lie in a $T$ range below that at which we can evaluate equilibrium liquid properties with current computational resources. However, several trends suggest a connection.

First, we find that the $T$ at which the peak of $C_V$ occurs decreases with increasing $\rho$, and passes outside of our range of observation at the approximate $\rho$ where liquid-liquid phase separation is proposed (Fig. 18). This behavior is consistent with the observed $C_V$ peaks being a line (in the $V$-$T$ plane) of high-$T$, non-singular thermodynamic anomalies that becomes singular as the critical region of the liquid-liquid transition is approached.

Second, the observed line of $C_V$ peaks naturally defines a "crossover zone" in the behavior of the liquid between a high-$T$, high-$\rho$ region (Region I in Fig. 18), within which the liquid is more fragile, the IS energies are relatively high, the tetrahedral network is disrupted, and the properties are in general more similar to simpler liquids; and a low-$T$, low-$\rho$ region (Region II in Fig. 18) within which the liquid is becoming strong, the IS energies are dropping (perhaps toward a lower limit), the tetrahedral network is becoming prominent, and complex thermodynamic behavior (e.g. negative expansivity) emerges. It is possible that these two regions of behavior, as $T$ decreases, become progressively more sharply separated, perhaps ultimately by a first-order phase transition.

More research, both through experiments and simulations, is required to confirm or refute such a picture. However, our current understanding of the BKS system suggests that three distinct phenomena may in fact be interrelated: (i) the FSC, (ii) polyamorphism, and (iii) the landscape behavior that allows the Kauzmann paradox to be avoided. In this regard, Sasai has recently studied the interrelationship of the FSC and a liquid-liquid phase transition in a random energy model [47]. Also, it is worth considering the behavior of other systems (e.g. $BeF_2$ [45]) that display one or more of the above three phenomena, to test if the others also appear. In particular, for any system that becomes strong at low $T$ via a FSC, it may be that polyamorphism can be observed under nearby thermodynamic conditions. This may be a useful clue for identifying polyamorphic materials.

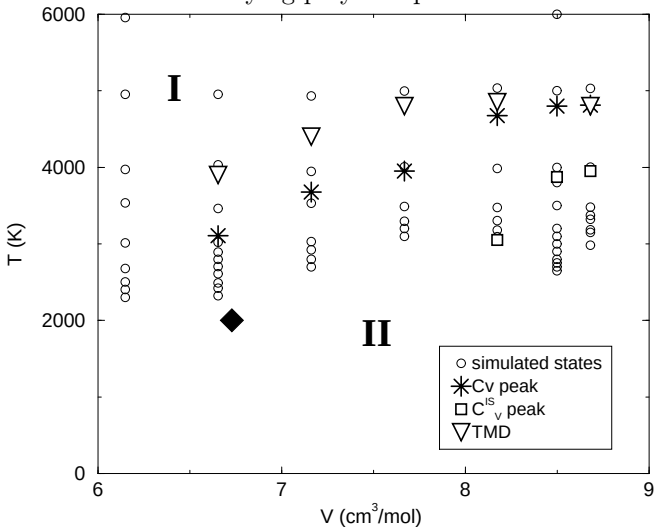


FIG. 18: Location of the line of $C_V$ maxima (asterisks) in the $V$-$T$ plane. Also shown are points on the "temperature of maximum density" (TMD) line (triangles), at which the isobaric expansivity changes sign; and the location of maxima in the contribution of $e_{IS}$ to $C_V$ (squares). The diamond indicates where evidence for liquid-liquid phase separation was found in Ref. [46]. The regions labeled I and II are referred to in the text.

## V. ACKNOWLEDGMENTS

We thank C.A. Angell, W. Kob, S. Sastry and R. Speedy for discussions. I.S.-V. and P.H.P thank NSERC (Canada) for funding and SHARCNET for computing resources and funding. P.H.P. also acknowledges the support of the Canada Research Chairs Program. F.S. acknowledges support from the INFM "Iniziativa Calcolo Parallelo" and PRA-HOP and from MIUR FIRB and PRIN 2000.

[1] C.A. Angell, J. Non-Cryst. Solids **131-133**, 13 (1991).
[2] P. Richet, Geochimica et Cosmochimica Acta **48**, 471 (1984).
[3] J. Horbach and W. Kob, Phys. Rev. B **60**, 3169 (1999).
[4] B.W.H. Van Beest, G.J. Kramer and R.A. van Santen, Phys. Rev. Lett. **64**, 1955 (1990).
[5] E. La Nave, H.E. Stanley and F. Sciortino, Phys. Rev. Lett. **88**, 035501 (2002).
[6] E.A. Jagla, Mol. Phys. **99**, 753 (2001).
[7] W. Götze, J. Phys.: Condens. Matter **11**, A1 (1999).
[8] A. Rinaldi, F. Sciortino and P. Tartaglia, Phys. Rev. E **63**, 061210 (2001).
[9] S. Mossa, E. La Nave, H.E. Stanley, C. Donati, F. Sciortino and P. Tartaglia, Phys. Rev. E **65**, 041205 (2002).
[10] Ashwin S.S. and S. Sastry, J. Phys.: Condens. Matter

**15**, S1253 (2003).
[11] M. Mézard and G. Parisi, Phys. Rev. Lett. **82**, 747 (1999).
[12] X. Xia and P.G. Wolynes, Phys. Rev. Lett. **86**, 5526 (2001).
[13] J.P. Garrahan and D. Chandler, Phys. Rev. Lett. **89**, 035704 (2002).
[14] M. Goldstein, J. Chem. Phys. **51**, 3728 (1969).
[15] F.H. Stillinger and T.A. Weber, Science **225**, 983 (1984).
[16] F.H. Stillinger, Science **267**, 1935 (1995).
[17] S. Sastry, P.G. Debenedetti and F.H. Stillinger, Nature **393**, 554 (1998).
[18] F. Sciortino, W. Kob and P. Tartaglia, Phys. Rev. Lett. **83**, 3214 (1999).
[19] S. Buechner and A. Heuer, Phys. Rev. E **60**, 6507 (1999).
[20] A. Scala, F. Starr, E. La Nave, F. Sciortino and H.E. Stanley, Nature **406**, 166 (2000).
[21] S. Sastry, Nature **409**, 164 (2001).
[22] L.-M. Martinez and C.A. Angell, Nature **410**, 663 (2001).
[23] P.G. Debenedetti and F.H. Stillinger, Nature **410**, 259 (2001).
[24] F.W. Starr, S. Sastry, E. La Nave, A. Scala, H.E. Stanley and F. Sciortino, Phys. Rev. E **63**, 041201 (2001).
[25] E. La Nave, F. Sciortino, P. Tartaglia, C. De Michele and S. Mossa, J. Phys.: Condens. Matter **15**, S1085 (2003).
[26] E. La Nave, S. Mossa and F. Sciortino, Phys. Rev. Lett. **88**, 225701 (2002).
[27] F. Sciortino and P. Tartaglia, Phys. Rev. Lett. **86**, 107 (2001).
[28] S. Mossa, E. La Nave, F. Sciortino and P. Tartaglia, Eur. Phys. J. B **30**, 351 (2002).
[29] A. Saksaengwijit, B. Doliwa and A. Heuer, J. Phys.: Condens. Matter **15**, S1237 (2003).
[30] G. Adam and J.H. Gibbs, J. Chem. Phys. **43**, 139 (1965).
[31] I. Saika-Voivod, P.H. Poole and F. Sciortino, Nature **412**, 514 (2001).
[32] MDCSPC2 is a MD program written by W. Smith, Daresbury Laboratory, UK. This program is distributed by the CCP5 Project via www.ccp5.ac.uk.
[33] Y. Guissani and B. Guillot, J. Chem. Phys. **104**, 7633 (1996).
[34] K. Vollmayr, W. Kob and K. Binder, Phys. Rev. B **54**, 15808 (1996).
[35] M.P. Allen and D.J. Tildesley, *Computer Simulation of Liquids* (Oxford University Press, Oxford, 1989).
[36] R.K. Pathria, *Statistical Mechanics* (Butterworth-Heinemann, Bodmin, U.K., 1996).
[37] W.H. Press, S.A. Teukolsky, W.T. Vetterling, and B.P. Flannery, *Numerical Recipes* (Cambridge University Press, Cambridge, 1992).
[38] M. Mezei and D.L. Beveridge, Annals of the New York Academy of Sciences **482**, 1 (1986).
[39] P.J. Heaney, Reviews in Mineralogy **29**, 1 (1994).
[40] N.R. Keskar and J.R. Chelikowsky, Phys. Rev. B **46**, 1 (1992).
[41] J.R. Smyth, J.V. Smith, G. Artioli and A. Kvick, J. Chem. Phys. **91**, 988 (1987).
[42] W. Kauzmann, Chem. Rev. **43**, 219 (1948).
[43] S. Corezzi, D. Fioretto and P. Rolla, Nature **420**, 653 (2002).
[44] M.S. Shell, P.G. Debenedetti and Z. Panagiotopoulos, Molecular structural order and anomalies in liquid silica, Phys. Rev. E **66**, 011202 (2002).
[45] M. Hemmati, C.T. Moynihan and C.A. Angell, J. Chem. Phys. **115**, 6663 (2001).
[46] I. Saika-Voivod, F. Sciortino and P.H. Poole, Phys. Rev. E **63**, 011202 (2001).
[47] M. Sasai, J. Chem. Phys. **118**, 10651 (2003).